Nature of the Surface Crossing Process in Bacteriorhodopsin: Computer Simulations of the Quantum Dynamics of the Primary Photochemical Event

A. Warshel* and Z. T. Chu

Department of Chemistry, University of Southern California, University Park Campus, Los Angeles, California 90089-1062

Received: February 22, 2001; In Final Form: June 17, 2001

The quantum dynamics of the primary photoisomerization event in bacteriorhodopsin is studied by a semiclassical trajectory approach. The relevant surface crossing probability is evaluated from the wave functions and potential surfaces of a hybrid quantum mechanical/molecular mechanics (QM/MM) Hamiltonian of the complete chromophore−protein−solvent system. The QM/MM model combines consistently the quantum mechanical Hamiltonian of the chromophore with the microscopic electric field of the ionized groups and induced dipoles of the protein−solvent system. The QCFF/PI Hamiltonian of the chromophore is adjusted to reproduce relevant ab initio results. The nonadiabatic coupling term $<\psi_1|\partial\psi_0/\partial t>$ is calculated numerically from the corresponding wave functions. The simulations are performed by combining the ENZYMIX and QCFF/PI molecular modeling programs. The effect of the protein on the absorption spectrum of the chromophore is examined. It is found that this spectrum reflects the effect of the protein permanent dipoles, ionized residues, water molecules (in and around the protein), and the induced dipoles of the protein plus water system. Next, we probe the motion along the excited state surface. It is demonstrated, in agreement with our early study and more recent works, that the motion starts with bond vibrations and evolves to a torsional motion. It is also found that we are dealing with an overdumped motion. Major emphasis is placed on the nature of the surface crossing process. In particular, we try to examine the origin of the very large probability of crossing in the $\pi/2$ region. A large crossing probability was obtained first in our early simulation (Warshel, A. *Nature* **1976**, *260*, 679), but its origin was not explored in details. Such large crossing probabilities can be obtained by passing through strict conical intersections (where the two surfaces "touch" each other) or by passing through regions with large nonadiabatic coupling and small energy gap (such regions are usually close to conical intersections). It is found that some trajectories pass through strict conical intersections, whereas others cross through regions with nonzero energy gap and a large nonadiabatic coupling. This feature helps probably to ensure the stability of the photobiological process with regards to various mutations. The average surface crossing probability and our previously derived expression (Weiss, R. M.; Warshel, A. *J. Am. Chem. Soc*. **1979**, *101*, 6131) appear to provide an excellent approximation for the calculated quantum yield. Furthermore, the calculated quantum yield reproduces the corresponding observed value. Finally, we examine the behavior of trajectories that cross to the ground state before the $\pi/2$ region. Our finding that these trajectories are deflected backward allow us to exclude models where the surface crossing occurs before the $\pi/2$ region.

I. Introduction

The light-induced reactions of rhodopsin and bacteriorhodopsin (bR) present some of the fastest and most efficient processes in biology (e.g., see refs 1−3). In both cases, the light energy leads to a very fast photoisomerization and most probably to storage of electrostatic energy,[1,4,5] which is then used to drive the specific biological process (i.e., visual excitation and proton pumping for rhodopsin and bR, respectively). The detailed nature of this ultrafast reaction is of significant interest, both as a unique photobiological process and as a challenge for theoretical studies. In particular, one would like to understand the quantum dynamics of the primary event and the role of the protein in optimizing the quantum yield of the photoisomerization reactions. The first simulation of the quantum dynamics of rhodopsin was reported in 1976.[6] This was accomplished by performing semiclassical molecular dynamics (MD) simulations of the surface crossing process in a model composed of a protonated Schiff base of retinal (PSBR) and a constraint that represented the steric effect of the protein. These calculations considered the complete Cartesian space of the given molecular model and predicted a photoisomerization time of ∼150 fs and a crossing probability of ∼30%. The predicted simulation time was much shorter than the experimental estimate at that time[7] (<6 ps). Subsequent time-resolved experiments[3,8−13] observed a photoisomerization time of ∼100−200 fs for rhodopsin and bR, which is in the range of the theoretical prediction. Several simulation studies of the photoisomerization process in rhodopsin and bR were reported[1,14−19] since the early work of ref 6. However, these instructive studies left major questions open. The studies of Birge and co-workers[14,15,20] used basically a one-dimensional model, assuming the rate of the vibrational relaxation rather than calculating it (see section III). Furthermore,

* To whom correspondence should be addressed.

10.1021/jp010704a CCC: $20.00
Published on Web 09/21/2001

the early models of these authors (e.g., see refs 14 and 20) used a constant electronic coupling term. Recent studies of Schulten and co-workers[18] included the protein in the simulations but assumed (rather than calculated) the form of the potential surfaces for the 13−14 torsional angle. Although this model produced reasonable intramolecular relaxation (vibrational relaxation), it did not involve a consistent coupling between the chromophore and the protein electric field, and most importantly it assumed the magnitude of the coupling between the electronic states rather than calculated it (see below). This makes it impossible to resolve some of the open questions about the primary event. The simulations of Warshel and co-workers[19] used a quantum mechanical/molecular mechanics (QM/MM) potential surface that treated the coupling between the chromophore and the protein consistently. However, this work only explored the intramolecular energy relaxation on the excited electronic state and did not calculate the surface crossing probability. Thus, it is not clear whether the picture that emerges from our early 1976 simulations would remain valid with a more complete representation of the protein.

The nature of the surface crossing process has been one of the most interesting open questions in the field. To address this problem in a clear way, it is useful to start from the considerations of Weiss and Warshel,[21] who tried to rationalize the origin of the high quantum yield in rhodopsin. These authors started from a semiclassical trajectory formulation and obtained the general expression (see also section II).

$$Y = (1 - f)/(2 - \theta) \tag{1}$$

Here Y is the quantum yield, θ is the average crossing probability, and f is the fraction of the system that does not reach the crossing point because of fluorescence or the other relaxation processes. Because the observed quantum yield is ~ 0.64,[22−24] it was concluded that θ is very large (~ 0.5), which means that about half of the trajectories cross every time they arrive at the $\pi/2$ region of the angle that undergoes an isomerization. This proposal has been quite different from the previously assumed picture that invoked equilibration at the excited state of the crossing region (e.g., see refs 25 and 26). The large value of θ was justified by finding a large value for the electronic coupling, $\sigma_{0,1}$, between the first excited state, ψ_1, and the ground state, ψ_0. A related proposal was introduced in the pioneering study of Michl,[27] who predicted the existence of "funnels" for some photochemical reactions. Michl's insightful prediction did not involve, however, a time dependent formulation and thus has not been given in terms of the relationship between the crossing probability θ and quantum yield (eq 1). At any rate, our early simulations have provided effectively a funnel for the photochemistry of rhodopsin, and the question we like to address now is whether this funnel picture is still valid and what is its origin.

Recent works of Robb, Olivucci, Bernadi, and their co-workers[28,29] have indicated that many photochemical reactions involve extremely fast singlet−singlet crossing, which is mediated through conical intersections. This fascinating phenomenon, see, for example, refs 30 and 31, involves cases where two adiabatic states actually cross each other (refs 30 and 32) so that they have a zero effective coupling and zero energy gap at the crossing point. The relevance of this idea to rhodopsin and bR is not yet clear because of enormous difficulties of evaluating the crossing process by high level ab initio methods. Ab initio calculations on the 2-*cis*-penta-2,4-dieniminium ion (CH_2═$CHCH$═$CHCH$═NH_2^+) referred to here as PDI,[33] a simple model of PSBR, found a conical intersection at a point where the central double bond was twisted by about 80°. This ab initio excited-state surface was much steeper than the surface obtained by semiempirical calculations. However, subsequent ab initio calculations on 4-*cis*-γ-methylnona-2,4,6,8-tetraeniminium ion,[34] a longer chromophore (referred to here as MNTI) which is probably a more realistic model of the visual pigment, has found that the excited-state surface approaching the intersection is much flatter than that obtained for 2-*cis*-penta-2,4-dieniminium. This study found that there is probably a conical intersection at $\pi/2$. It is not clear, however, whether a strict conical intersections with $\Delta E = 0$ can be reached by all actual trajectories of MNTI or bR. It is possible that the surface crossing in rhodopsins involves cases with large electronic coupling (large $\sigma_{0,1}$) which do not involve actual $\Delta E = 0$. Such cases might still reflect the existence of a nearby conical intersections.[35] However, from our perspective, the issue is whether the previous 1976 picture of a funnel with energy gaps of $\Delta E \leq 6$ kcal/mol and large $\sigma_{0,1}$ is still valid (rather than the possibility that this picture reflects the neighboring of conical intersections). Thus, we will introduce here an arbitrary separation between cases of strict conical intersections or their immediate regions (say $\Delta E \leq 2$ kcal/mol) and cases with larger ΔE's. With this separation in mind, we will try to evaluate the relative contributions from the two limiting cases.

Resolving the true nature of the quantum dynamics of rhodopsins can be accomplished (at least in principle) by a semiclassical trajectory treatment with potential surfaces, which are based on a high level ab initio QM/MM Hamiltonian. However, such a treatment, with a sufficient number of trajectories, is too expensive at the present time. In the current work, we adopt a more practical alternative using a QM/MM approach with the semiempirical QCFF/PI method. This method which was used in the original 1976 work, includes now the complete effect of the protein−solvent environment (as was done in our study of the excited-state dynamics of bR[19]). The QCFF/PI surfaces are recalibrated to reproduce the trend of the ab initio studies of refs 33 and 34. The calibrated QM/MM surface is used to further clarify the quantum dynamics of rhodopsin-type systems. The specific system we have decided to study is bR, because a relatively high-resolution structure of the protein is now available.[36−39]

Section II describes the semiclassical method used and the corresponding potential surfaces. Section III describes the results of the simulations focusing on the motion toward the crossing region, the nature of the crossing process, and the quantum yield. Finally, we discuss in section IV the significance of our findings.

II. Methods

II.1. Semiclassical Surface Crossing Treatment. Our task is to simulate the quantum dynamics and quantum yield in bR. The options available include the semiclassical trajectory approaches,[6,40,41] density matrix treatments,[42] and related treatments (e.g., see ref 18). The semiclassical trajectory approach was originally formulated for studies of gas-phase reactions of systems with a few atoms.[40,41] However, this method has been found to be particularly useful for reactions of large molecules[6,43] and reactions in condensed phases.[44−46] In this approach, one treats the nuclear motion classically, while evaluating the probability of being at different electronic states quantum mechanically (see below). Although this treatment is clearly an approximation, it helps one to keep a proper physical insight, which is crucial in treating complex systems. In the present work, we follow the same semiclassical approach that was used in our original study[6] and whose main features are discussed below.

Let us consider the crossing probability from the lowest excited singlet state to the ground state, when the higher singlet states are at a sufficiently high energy above the lowest excited state. In this case, we can describe the time dependent wave function of our system by

$$\Psi(\mathbf{r},t) = a_0(t)\psi_0(\mathbf{r}) \exp\{-i\hbar\int_0^t E_0\, dt'\} + a_1(t)\psi_1(\mathbf{r}) \exp\{-i\hbar\int_0^t E_1\, dt'\} \quad (2)$$

where $|a_0(t)|^2$ and $|a_1(t)|^2$ are the corresponding probabilities that the system will be in the ground and the first excited state at a time t. The $\psi(\mathbf{r})$'s and E's are, respectively, the time independent adiabatic wave functions and energies. Using the time-dependent Schrödinger equation

$$H(\mathbf{r})\Psi(\mathbf{r},t) = i\hbar\, \partial\Psi(\mathbf{r},t)/\partial t \quad (3)$$

one obtains

$$a_0(\tau) = -\int_0^\tau \sigma_{0,1}(t)a_1(t) \exp\{-i\int_0^t \Delta W(r(t'))\, dt'\}\, dt$$

$$a_1(\tau) = -\int_0^\tau \sigma_{1,0}(t)a_0(t) \exp\{i\int_0^t \Delta W(r(t'))\, dt'\}\, dt \quad (4)$$

where the transition amplitudes (the a_i) have a real and an imaginary component, the coupling term $\sigma_{1,0}$ is given by $\sigma_{1,0} = \langle\psi_1|\partial\psi_0/\partial t\rangle$, and $\Delta W = (E_1 - E_0)/\hbar$. Equation 4 can be evaluated semiclassically by using the time dependent coordinate vector, $\mathbf{r}(t)$, [and the corresponding $\Delta W(r(t))$] obtained by running classical trajectories on some combination of E_1 and E_2 (see below). The value of $|a_0|^2$ and $|a_1|^2$ can be used to determine the probability of being in the ground and the excited state, respectively. More specifically, in studies of cis−trans photoisomerization reaction, we start in the Franck−Condon region of the excited state with $\mathrm{Re}[a_1(0)] = 1$, $\mathrm{Im}[a_1(0)] = 0$, $\mathrm{Re}[a_0(0)] = 0$, and $\mathrm{Im}[a_0(0)] = 0$ and start to run a trajectory $\mathbf{r}_1(t)$ on E_1. The trajectory is propagated until a point where ΔW reaches a minimum value. At this time, $\tau_0^{(1)}$, the trajectory splits to two branches: one branch $\mathbf{r}_1(t)$ jumps to E_0 on some effective potential that guaranties conservation of energy (see below), whereas the other, $\mathbf{r}_2(t)$, continues on E_1. The probability of being on $\mathbf{r}_1(t)$ and arriving to the ground state is taken as $P_1 = |a_0(r_1(\tau_0^{(1)} + \Delta\tau_1))|^2$, where the integration of eq 4 along $\mathbf{r}_1(t)$ continues until a time, $\tau_0^{(1)} + \Delta\tau_1$, in which ΔW reaches a maximum value. The second branch of the trajectory, $\mathbf{r}_2(t)$, continues from $\tau_0^{(1)}$ on E_1 and the probability of being on this trajectory is taken as $(1 - P_1)$. This division of probabilities makes the essential assumption that interference between the amplitudes of the probabilities of being on different trajectories can be neglected (a detailed justification of this crucial assumption is given in ref 45). Now, we have to keep monitoring $\mathbf{r}_2(t)$, which represents the fraction of the system which is still on the excited state. To do so, we follow this trajectory up to the next turning point on E_1 and reset $|a_0(\mathbf{r}_2(t))|$ to zero and $|a_1(\mathbf{r}_2(t))|$ to one. When $\mathbf{r}_2$ arrives again at the crossing point, $\tau_0^{(2)}$, we once more split the trajectory to $\mathbf{r}_2$ and $\mathbf{r}_3$. Now, $\mathbf{r}_2$ is allowed to cross to E_0 with a probability $P_2 = (1 - P_1)|a_0(\mathbf{r}_2(\tau_0^{(2)} + \Delta\tau_2))|^2$, whereas $\mathbf{r}_3$ continues on E_1 and so on. The probability of being at different regions of the ground state is evaluated as the sum of the probabilities of finding the corresponding branches of trajectories. Thus, we have

$$\bar{P}_{\mathrm{cis}} = \sum_{i=1} P_i(r_i)(\delta_{i,\mathrm{cis}})$$

$$\bar{P}_{\mathrm{trans}} = \sum_{i=1} P_i(r_i)(\delta_{i,\mathrm{trans}}) \quad (5)$$

where $\delta_{i,\mathrm{cis}}$ is 1 where r_i ends at the cis region and zero when r_i ends at the trans region. $\delta_{i,\mathrm{trans}}$ is defined similarly. A trajectory is considered to end in the cis (trans) if it continues immediately after the crossing toward this direction. This implies that once a trajectory starts to move in the cis (trans) direction it will relax at this ground-state region. This treatment should, in principle, be corrected by considering the chance that a trajectory that cross in the cis (trans) direction will be deflected back to the trans (cis) direction, see section III.4. At any rate, the simulation procedure described above should be repeated by starting many trajectories from different points at the initial Franck−Condon region of the excited state and evaluating the quantum yield for each of these simulations. Averaging the quantum yields of the different simulations should provide the actual quantum yield of the system under study.

Semiclassical trajectory approaches require one to select the proper effective nuclear potential. This problem has been addressed by several workers (e.g., see refs 46−48) and will be also examined here in a qualitative way. Probably the most important aspect of this issue is how to continue the trajectory at the crossing point. Here, one may try to guarantee the conservation of energy by using the approximation proposed by Miller and George.[40] However, this formulation does not seem to hold for cases where the change in potential energy, ΔW, is larger than the initial kinetic energy (i.e., $\Delta W > 0.5\mathbf{p}^{(1)}M^{-1}\mathbf{p}^{(1)}$ in the notation of ref 40). Thus, we introduce a more straightforward numerical procedure, to satisfy the requirement that the change in kinetic energy is equal to ΔW. That is, we start by noting that the above requirement can be written as

$$\frac{1}{2}(\mathbf{p}^{(2)}M^{-1}\mathbf{p}^{(2)} - \mathbf{p}^{(1)}M^{-1}\mathbf{p}^{(1)}) = \Delta W \quad (6)$$

where M is the mass matrix in the Cartesian representation (in this representation it is a diagonal matrix) while $\mathbf{p}^{(1)}$ and $\mathbf{p}^{(2)}$ are the nuclear momenta on E_1 and E_0, respectively. ΔW is the difference between the potential surface E_1 and E_0 at the crossing point. Now, we use

$$\mathbf{p}^{(2)} = \mathbf{p}^{(1)} + \beta\mathbf{n}(\mathbf{n}M^{-1}\mathbf{p}^{(1)}) \quad (7)$$

where $\mathbf{n}$ is a unit vector normal to the surface of the avoided intersection (see also ref 40). In our procedure, β is the numerically adjusted parameter, which is increased gradually until the resulting $\mathbf{p}^{(2)}$ satisfies eq 6. When we find the proper β, we are guaranteed that the change in kinetic energy upon crossing is equal to ΔW.

Although our simulations involve the complete dimensionality of the system studied, it is instructive to have some insight from a simplified one-dimensional treatment. For simplicity, let us consider the electronic states of a typical PSBR as a function of the double bond which undergoes an isomerization (Figure 1). In this case, if we start with $\mathrm{Re}[a_1(0)] = 1$, $\mathrm{Im}[a_0(0)] = 0$, $\mathrm{Re}[a_0(0)] = 0$, and $\mathrm{Im}[a_0(0)] = 0$, eq 4 becomes

$$|a_0(\tau)|^2 = |\int_0^\tau \sigma'_{0,1}(\phi)\dot{\phi}a_1(t) \exp\{-i\int_0^t \Delta W(\phi(t'))\, dt'\}\, dt|^2 \quad (8)$$

where ϕ is the torsional angle, $\dot{\phi} = \partial\phi/\partial t$, $\sigma' = \partial\sigma/\partial\phi$, and $\sigma(t)$

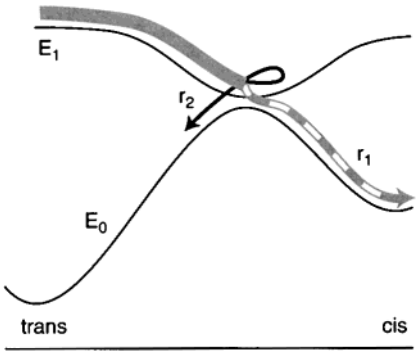

Figure 1. Schematic description of the ground, E_0, and the first excited, E_1, states that are involved in the photoisomerization of bR. The figure also depicts a trajectory that moves on the excited state up to the $\pi/2$ region and then splits to two trajectories: one, r_1, crosses to the cis direction of E_0 and the other, r_2, continues on E_1 and then crosses to the trans direction.

is replaced by $\sigma'(\phi)\dot{\phi}$ (we keep in mind that the transition amplitudes have both real and imaginary components). The change of ϕ with time can be obtained from trajectories calculations for the molecule under consideration. In general, a trajectory reaches the $\pi/2$ region with a velocity $\dot{\phi}_0$, and then a fraction, θ, crosses to the ground state. The average value of θ is given by

$$\theta = \langle |a_0(\tau_0 + \Delta\tau)|^2 \rangle \cong \langle | \int_0^{\tau_0+\Delta\tau} \sigma'_{1,0}(\phi)\dot{\phi} a_1(t) \exp\{-i\int_0^t \Delta W(\phi(t'))\, dt'\}\, dt|^2 \rangle \quad (9)$$

where τ_0 is the time of arrival to $\pi/2$ and most of the crossing ends at the time $\tau_0 + \Delta\tau$. Note that our θ is the above-mentioned $P_1(r_1)$. Here, we have designated by $\langle\ \rangle$ an average over different excited trajectories that start at $t = 0$ from the Franck−Condon region with different initial conditions (generated by exciting the ground state). Because only regions with small ΔW contribute to θ, one can expand $\Delta W(t)$ about the time where $\phi = \pi/2$ (where ΔW reaches its minimum value) and obtain

$$\Delta W(t) \cong \Delta W(\tau_0) + \Delta\ddot{W}\Delta t^2/2 \cong \Delta W_0 + (\partial^2\Delta W/\partial\phi^2)_0\, (\dot{\phi}_0{}^2\Delta t^2)/2 \quad (10)$$

Using $\Delta t = t - \tau_0 = [(\phi(t) - \pi/2)/\dot{\phi}_0] = (\Delta\phi/\dot{\phi}_0)$, the integral in the phase in eq 9 can be written as

$$\int_0^t \Delta W(t')\, dt' = \int_0^{\tau_0} \Delta W(t')\, dt' + \Delta W_0\Delta t + \frac{1}{6}\Delta\ddot{W}_0\Delta t^3 = \int_0^{\tau_0} \Delta W(t')\, dt' + (\Delta W_0/\dot{\phi}_0)\Delta\phi + \Delta W''_0(\Delta\phi^3/\dot{\phi}_0)/6 \quad (11)$$

where $\Delta W'' = (\partial^2\Delta W/\partial\phi^2)_0$ and $\ddot{W}_0 = (\partial^2\Delta W/\partial t^2)_0$.

Now, eq 9 can be approximated by

$$\theta = |\int_{\phi_0-\Delta\phi_1}^{\phi_0+\Delta\phi_1} \sigma'_{1,0}(\phi) \exp\{-i(\Delta W_0/\dot{\phi}_0)\Delta\phi + \Delta W''_0(\Delta\phi^3/\dot{\phi}_0)/6\}\, d\phi|^2 \quad (12)$$

where $\phi_0 = \pi/2$ and $\Delta\phi_1 = \Delta\tau\dot{\phi}_0$. Note that the term $\int\Delta W$ in eq 11 disappears when taking the absolute value of a_0. In the range of a dumped oscillatory motion, which seems to be appropriate to our case (see below), the average value of θ should not depend strongly on whether we are at the first pass or in subsequent passes at the $\pi/2$ region. In this case, we obtain the Weiss Warshel (WW) semiclassical expression for the quantum yield (see ref 21).

$$Y = \bar{P}_{cis}/[\bar{P}_{cis} + \bar{P}_{trans}] = (1 - f)[\theta + \theta(1 - \theta)^2 + \theta(1 - \theta)^4 + ...] = (1 - f)/(2 - \theta) \quad (13)$$

where f is the fraction of the system that does not reach the crossing point (e.g., the fraction lost by florescence). This relationship gives a much more realistic physical insight than that obtained from earlier treatments which described the photoisomerization process by the general theory of radiationless transitions (e.g., see refs 49−52). For example, it is hard to rationalize the high quantum yield of rhodopsin by such approaches. That is, according to the theory of radiationless transitions the rate constant for the decay of an excited state is proportional to $\exp\{-\Delta E^0_{0,1}\}$, where $\Delta E^0_{0,1}$ is the energy gap between the minima of the ground and excited states. Because the resting protein specifically binds a particular isomer (11-cis in rhodopsin and all-trans in bR), $\Delta E^0_{0,1}$ is larger for this isomer than for the product of the photoisomerization (all-trans rhodopsin or 13-cis bR). The energy-gap law would thus predict a much lower quantum yield in the reverse reaction than in the forward reaction.

The apparent failure of the energy-gap law in rhodopsin and bR can be ascribed to the wave packet behavior of the system. In a simple, but physical consistent semiclassical picture, the quantum yield depends on the momentum of the wave packet (or the corresponding classical trajectory) in the crossing region and gives the quantum yield of eq 13. Here, the simple semiclassical picture offers an excellent insight.

The magnitude of θ depends on the coupling term, $\sigma_{1,0}(t)$. This term is given by

$$\langle\psi_1|\partial\psi_0/\partial t\rangle = \langle\sum_N C_{1,N}\Phi_N\, (\partial/\partial t \sum_{N'} C_{0,N'}\Phi_{N'})\rangle = \sum_N C_{1,N}\dot{C}_{0,N} + \sum_{N\neq N'} C_{1,N}C_{0,N}\langle\Phi_N|\dot{\Phi}_{N'}\rangle \quad (14)$$

where the Φ_N's are the Slater determinants for the Nth configuration. These Φ_N's include the ground state and the singly excited and the doubly excited configurations. The matrix elements $\langle\Phi_N|\dot{\Phi}_N\rangle$ are reduced to molecular orbital matrix elements $\langle\phi_m|\dot{\phi}_{m'}\rangle$ (the molecular orbitals are given by $\phi_m = \sum_k v_{mk}\lambda_k$ where the λ's are the Löwdin orbitals for the π atoms). Finally, the matrix elements $(\phi_m|\dot{\phi}_{m'})$ are expressed as the product of the corresponding vectors of the molecular orbitals coefficient $(\mathbf{v}_m\cdot\dot{\mathbf{v}}_{m'})$ (the "selection rules" here are identical to that of transition dipoles[53]). The time derivative of $\dot{C}$ and $\dot{\mathbf{v}}$ are evaluate by a numerical differentiation along the given trajectory. This procedure, which is straightforward to implement in π electron calculations, has been used in our original work[6] and in our subsequent studies.[21]

Our early analysis of eq 13 (see ref 21) led to the conclusion that θ should be much larger than what was thought at that time, where it was frequently assumed that the system would equilibrate at the $\pi/2$ region.[25,26,54] Our conclusion was supported by calculation of the actual magnitude of σ. These considerations involved calculation of σ of retinal by the QCFF/PI model with a full single and double CI (Figure 1 of ref 21) and a simplified two-orbital Hückel model that allowed us to demonstrate the general trend. It was found that σ increases rapidly at the $\pi/2$ region and that this is an important factor in obtaining large θ. This finding was criticized by Persico and Bonacic-Koutecky,[26]

who incorrectly presumed that it was not obtained with a CI treatment (in contrast to the clear statement in Figure 1 of ref 21) and argued that σ does not change significantly at the $\pi/2$ region. They further argued that the coupling to the ground state is too small to compete with the thermal equilibration of the excited state.[26,54] A recent work of Tallent et al.[15] also assumed incorrectly that the study of Weiss and Warshel was confined to only two orbitals and thus obtained an overestimate of σ. At any rate, actual calculations supported the trend of our finding. First, at least one of the calculations reported by Persico and Bonacic-Koutecky (Figure 8 of ref 26) produced a relatively sharp increase in σ at the $\pi/2$ region and all calculations produced almost as large σ at $\pi/2$ as that obtained in ref 21 [$\sigma(\pi/2) \cong 2$ and $\sigma(\pi/2) \cong 4$ in refs 26 and 21, respectively]. Furthermore, the calculations of ref 26 were not done for highly polarized double bonds, as is the case of PSBR, but for propylene. We also note several more recent calculations[55,56] for PSBR obtained a σ with a sharp peak at $\pi/2$.

It might also be useful to comment here on the recent calculation of σ by Tallent et al.[15] These authors recognized the problems of using a constant σ in their previous studies (e.g., see ref 20) and tried to evaluate eq 4 with an actual calculation of σ. However, this still involved a serious approximation, because σ was calculated using only the highest occupied molecular orbital and the lowest unoccupied molecular orbital (rather than the actual states in the proper CI description).

Finally, it is instructive to note that the picture of large $\sigma_{1,0}$ and medium size $\Delta E'_{0,1}$ is quite consistent with being in the neighborhood of a conical intersection,[35] and both pictures should lead to large θ and to an effective 'funnel" for the surface crossing process.

II.2. Potential Surfaces. As stated in the Introduction, obtaining a practical and reliable QM/MM model for studies of the photoisomerization in bR or related molecules is far from obvious. Although high level ab initio calculations have been used in studies of the least energy path in model compounds,[29] they cannot yet be used in practical studies of bR because this would require enormous computer time. It seems to us that the most reliable option is to use a QM/MM version of QCFF/PI method as was done in our previous work[19] and to try to calibrate the corresponding surface to reproduce the available gas phase ab initio results. The present work uses a combination of the QCFF/PI quantum mechanical potential surface (see, for example, refs 57 and 58) and the protein force field of the program ENZYMIX.[59] The combined QCFF/SOL[60] program that combines the ENZYMIX and the QCFF/PI programs has been used in recent related studies of conjugated molecules in solutions.[60] The programs are available through our Web site. The main points about our potential surfaces and simulation approach are considered below.

The combined QM/MM potential surface for the Nth electronic excited state of the chromophore in its protein active site is expressed as

$$V^N(\mathbf{r}) = V^N_\pi(\mathbf{r}_S) + V_\sigma(\mathbf{r}_S) + V_{Ss}(\mathbf{r}_S,\mathbf{r}_s) + V_{ss}(\mathbf{r}_s) \quad (15)$$

where S and s designate, respectively, the "solute" (i.e., the chromophore) and the "solvent" which involves in our case the protein and its internal and surrounding water molecules. V^N_π is the π-electron contribution to the Nth excited state of the chromophore, V_σ is the σ-electron contribution to the chromophore surface. V_{Ss} is the potential that couples the protein (solvent) and the chromophore and V_{ss} is the protein force field of the protein and solvent system. The surfaces V_π and V_σ are obtained by the QCFF/PI method.[57,58] This method represents V^N_π by a PPP type approach (with Löwdin's corrections and a consistent treatment of the $\sigma-\pi$ coupling[57]), while representing V_σ by an empirical force field. The QCFF/PI method is well documented and widely available (e.g., see ref 61). This method has been used extensively in studies of retinal and related systems (e.g., see refs 58, 60, and 62) and is probably as reliable and far more efficient than the most advanced all-valence electron semiempirical approaches for treatments of medium size conjugated molecules (see, for example, ref 63).

The present study of bR includes in the QM region all the PSBR atoms. The QM treatment involves a configuration interaction treatment of all the single excitations, the double excitations of the type $ii \rightarrow jj$ for the three highest occupied and the three lowest unoccupied orbitals and the double excitations of the type $ij \rightarrow kk$ and $ii \rightarrow kj$ for the two highest occupied and the two lowest unoccupied orbitals. Adding more excitations appears to give similar results. The parameters used are those of ref 57. These parameters were already used in the early work of ref 6 and the corresponding excited-state surface of the 9−10, 11−12 torsional space has been described in detail in ref 5. This surface is quite similar to that obtained in a recent all-valence electron study of a related system.[55]

The solute−solvent coupling potential, V_{Ss}, is obtained by the approach introduced in ref 6 and described in detail in ref 60. This is done by incorporating the electrostatic potential from the solvent (or protein) in the solute Hamiltonian, using[60]

$$F_{\mu\mu} = F^0_{\mu\mu} - \sum_k (q_k/r_{k\mu} + \mathbf{m}_k\mathbf{r}_{k\mu}/r_{k\mu}{}^3) = F^0_{\mu\mu} - U_\mu$$

$$F_{\mu\nu} = F^0_{\mu\nu} \quad (16)$$

where $F^0_{\mu\nu}$ is the corresponding element of the solute's SCF matrix and k runs over the solvent atoms. q_k and $\mathbf{m}_k$ are respectively the residual charge and induced dipole on the kth atom of the solvent. Overall, the second term in $F_{\mu\mu}$ represents the potential U_μ, on the μth atom from its surrounding. The induced dipoles are evaluated self-consistently and are an important part of our treatment. The solute charges are evaluated in each MD step with the current elements of the **U** vector, which reflect the current solvent configuration, whereas the solvent molecules respond in each step to the solute charges in the electronic state whose surface drives the given MD simulation. The treatment of solvent and protein induced dipoles in the excited-state calculations is based on the procedure used in eq 17 of ref 60. In this approach, we allow the solvent permanent and induced dipoles to respond to the charge distribution of the electronic state that is being considered. Note that in this respect, that there is no QM/MM approach which provides a fully consistent treatment of the polarization of the solvent in each excited state (see the discussion in ref 60). Furthermore, a perturbation treatment which is very reasonable in some limits (see the Appendix of ref 60) does not provide results which are identical to those obtained by eq 17 of ref 60, where the induced dipoles are polarized differently in each electronic state (see, again, ref 60). At any rate, we believe that our explicit molecular treatment of the solvent induced dipoles is a useful step toward a realistic evaluation of excited states surfaces in proteins and solutions.

The solute−solvent interaction term of eq 15 also includes the classical van der Waals interactions between the solute and the solvent atoms as well as the bonding interaction for the bond between the chromophore and the lysine residues. The protein + solvent potential, V_{ss}, is represented by the ENZYMIX force

field (see ref 59) that includes the polarization constraints of the surface constrained all-atom solvent (SCAAS) model (see refs 59 and 64) and the local reaction field (LRF) long-range treatment.[65] The protein and solvent atoms within a simulation sphere of 22 Å, which is centered around C_{13} of the chromophore, are treated without any constraints, whereas the rest of the system is constrained by the SCAAS treatment (see ref 59). The protein coordinates are those reported in ref 39. The ionizable groups Asp 212, Asp 115, Asp 85, and Arg 82 are kept ionized during the simulations. The simulation sphere includes water molecules in the available cavities and around the protein. We believe that our treatment of the solvent molecules and long-range electrostatic effects are (at present) more reliable than other alternative treatments (at least we have examined the performance of our approach on many relevant test cases[66]).

Although the above potential surfaces are quite reasonable, it is important to try to calibrate them with the increasingly available high level ab initio results or the relevant experimental information. Effective calibration can be obtained by modifying the diagonal CI matrix elements using functions of the torsional angles. For examples, we can use

$$A^{N} = A_0^{N} + \sum_i B_i^{N} \cos\phi_i + C_i^{N}(\cos\phi_i)^2 + D_i^{N} \exp\{-(\phi_i - \phi_i^{0})^2/\alpha_i\} + F^{N} \quad (17)$$

where N runs over the different electronic configurations, i runs over all of the π bonds, A_0^{N} is the original QCFF/PI CI matrix element, and ϕ_i is the torsional angle around the ith bond of the chromophore. In this work, we chose to only modify the CI matrix element of the single excitation from the HOMO to the LUMO orbitals. For this matrix element, we set all of the coefficients in eq 17 to zero except those for the 13−14 bond. Thus, we used

$$A^{6\rightarrow 7} = A_0^{6\rightarrow 7} + 1.70\cos\phi_{13-14} + 0.65(\cos\phi_{13-14})^2 + 0.10\exp\{-(\phi_{13-14} - \pi)^2/0.30\} - 1.7 \quad (18)$$

where the contributions to $A^{6\rightarrow 7}$ are given in eV. The parameters in eq 18 were refined by fitting the QCFF/PI minimum energy path (MEP) for the isomerization around the 4th double bond of MNTI (this bond corresponds to the 13−14 bond of PSBR) to the corresponding CASSCF ab initio MEP.[29] The calibrated QCFF/PI MEP is compared to the ab initio MEP in Figure 2. As seen from the figure, we obtained a reasonable agreement between the two MEPs. We did not try to further improve the fitting in view of the sensitivity of the ab initio results to the method used.[67] This uncertainty is combined with the uncertainties about the effect of the environment. For example, using the parameters of eq 18 for bR we obtained conical intersections at $\phi < \pi/2$ and $\phi > \pi/2$ (rather than at $\phi = \pi/2$), and as will be shown in section III.5, this is a problematic result. Fitting to the CASPT2 of MNTI made this problem more serious. On the other hand, when we eliminated the induced dipoles correction, we obtained a reasonable result of a small energy gap at the $\pi/2$ region. However, the addition of the induced dipoles effect led to a large blue shift of the calculated spectrum of bR (relative to the corresponding observed spectrum). We expect that similar problems will appear in QM/MM approaches with ab initio Hamiltonians, when such approaches will become practical. Thus, we only view the calibrated surfaces as an approximated starting point and used the parameters in eq 18 as a toll for examining different limiting cases. With this in mind, we used

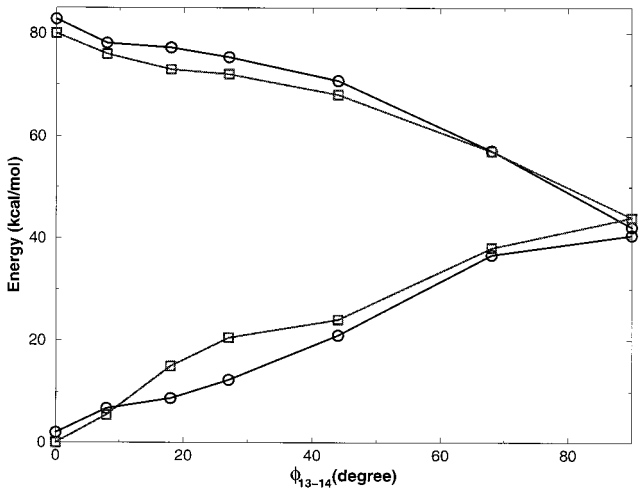

Figure 2. Ab initio (□) and calibrated QCFF/PI (○) potential surfaces for isomerization around the central double bond of MNTI. The ab initio results are taken from ref 34. The QCFF/PI energies for $\phi = 0$ were obtained by ground-state minimization, whereas all other points were obtained by an excited-state adiabatic mapping (where ϕ was fixed and the energy was minimized with respect to all other coordinates).

two sets of parameters. In the first set (which is referred to here as set I), we used the parameters of eq 18. In the second set (referred to here as set II), we changed B, C, and F to 0.97, 0.88, and −0.45, respectively. As will be shown below, the second set gives more reasonable results for the overall quantum yield.

At this point, we would like to put our treatment in a proper perspective. That is, although our treatment is not perfect, it takes into account the effect of the protein on the chromophore and represents the quantum mechanical coupling between the chromophore torsional angles. This is not done in recent alternative treatments (see the discussion in ref 68).

III. Results and Discussion

The X-ray structure of ref 39 was used as a starting point for a relaxation run of 20 ps in the ground-state all-trans system. This relaxation run was performed with 1 fs time steps and 300 °K, and the protein was solvated by the SCAAS model and treated by the LRF long-range treatment as implemented in the program ENZYMIX (see section II.2). The ground-state trajectories were used to generate the absorption spectrum (see section III.1) and to generate the initial conditions for the excited-state trajectories. The initial coordinates and momeda for the excited-state trajectories were generated by taking the coordinates and velocities from the ground-state trajectories on E_0, at time intervals of 2 ps, and then changing the surfaces from E_0 to E_1. This generated excited-state molecules in the Franck−Condon region. These initial geometries and momenta were used to simulate the excited-state dynamics with 0.02 fs time steps (such short time steps are needed for stable integration of eq 4 and stable evaluation of σ). The simulations allow us to generate a realistic description of the motion of the chromophore toward the crossing region as well as its crossing to the ground state. The corresponding trajectories were analyzed in different stages of their relaxation process, examining first the excited-state motion and then the crossing process. The results of this analysis are described below.

III.1. Absorption Spectrum of bR. The nature of the spectra of rhodopsins has been the subject of many experimental (e.g., see refs 69 and 70) and theoretical studies (e.g., see refs 1, 6, 71, and 72). Unfortunately, most previous theoretical works

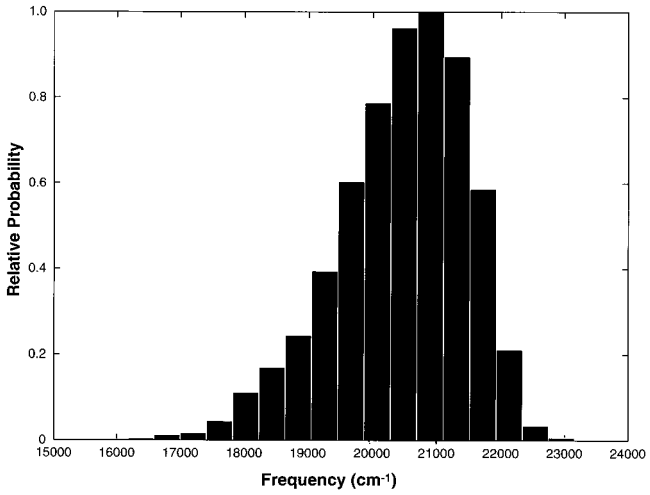

Figure 3. Calculated probability profiles for the excitation energies of the $\pi \rightarrow \pi^*$ transition in bR. The profile was obtained by running trajectories on the ground-state surfaces of the corresponding systems and evaluating the histograms of the calculated excitation energies.

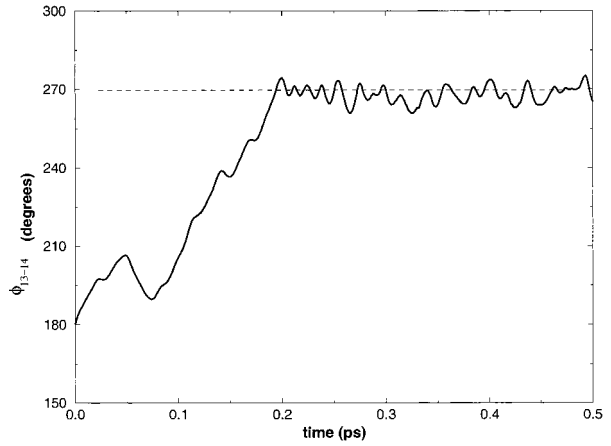

Figure 4. Time dependence of ϕ_{13-14} of bR for a trajectory that started at the Franck−Condon region of the excited state and was not allowed to cross to the ground state. As seen from the figure (see also ref 19), we have here a diffusive overdamped motion.

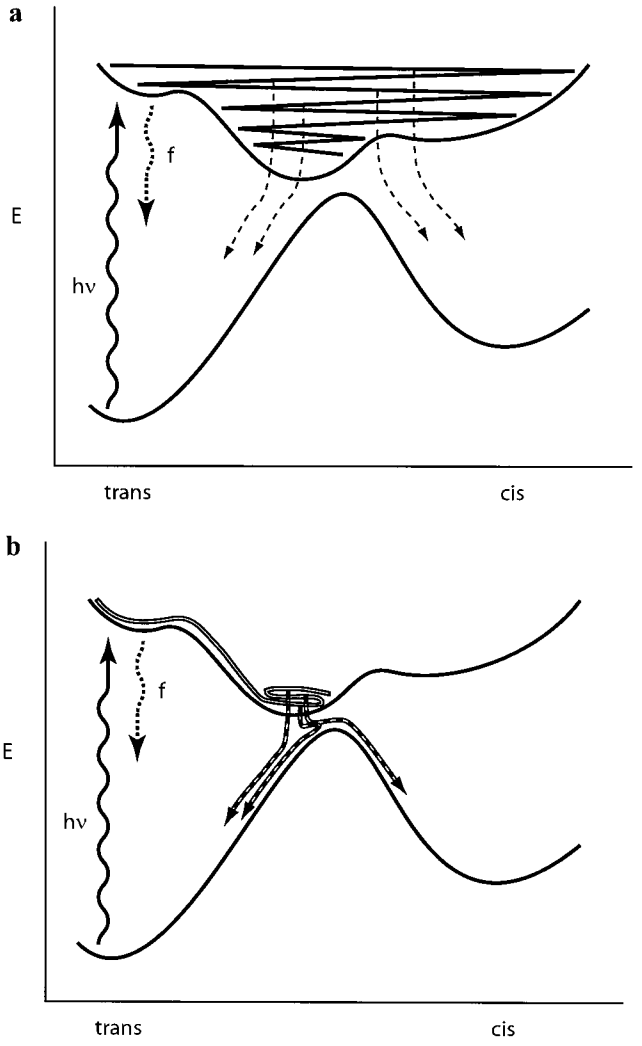

Figure 5. Schematic representation of two *inconsistent* limiting photoisomerization models where the minimum of the excited states is not at $\pi/2$. The figure considers the limiting cases of the inertial model (a) and the overdamped model (b) for the situation where the minimum of the excited state is shifted from the maximum of the ground-state surface. In the inertial model, we expect to get a significant trans → cis quantum yield even if the excited-state minimum is to the left of the ground-state maximum. However, our simulations exclude such an inertial model. In the limit b, one expects to obtain a very small quantum yield for the trans → cis isomerization, because most trajectories will end up in the trans group state. Because case a is not supported by the simulations and case b does not reproduce the observed quantum yield, it is clear that the potential surfaces cannot be described in the way depicted in this figure.

involve improper approximations. For example, most studies of the effect of the external charges (which were suppose to represent the effect of the protein ionized groups; e.g., see refs 1 and 72) did not treat properly the dielectric screening of the protein. Our preliminary studies[6,73] emphasized the fact that the calculated effect of external charges will be drastically reduced once the environment is properly considered. We also reported the first proper QM/MM calculations of the spectral shifts in several proteins (e.g., see refs 57 and 74) and the spectral shifts or retinal[60] and PSBP[75] in solution. Recent QM/MM calculations of the effect of mutations on the spectra of bR produced unstable results[71] and forced the authors to artificially omit large energy fluctuations. In the present work, we tried to exploit the stability of the QCFF/PI method and to evaluate the spectra of bR. This was done by running a 30 ps trajectory on the ground-state surface of bR, collecting the resulting energy gaps, and using the corresponding histograms as a rough estimate of the absorption spectrum. More systematic line shape analysis can be done by the dispersed polaron model (as was done in our previous work[60]), but this is out of the scope of the present work. The results of our simulations with the parameters of set I are shown in Figure 3. The calculated absorption maximum with this set is at ∼20 800 cm^{-1} as compared to the observed value of 17 543 cm^{-1}. The resulting spectrum reflects an intricate balance between several factors. This includes the effects of the protein permanent dipole (polar groups), the protein ionized residues, the internal and surrounding water molecules, and the induced dipoles of the protein plus water system. More specifically, omitting the induced dipoles, we obtained a blue shift of ∼1500 cm^{-1} (relative to the spectrum calculated with the induced dipoles), whereas omitting all of the external electrostatic effects produced a red shift of ∼600 cm^{-1}. It is important to note that the induced dipoles effect is missing in other theoretical studies of the spectrum of bR.

The present study did not examine the red shift of bR relative to the corresponding spectrum of PSBR in solution. We expect that QCFF/PI simulation will produce a larger blue shift in water

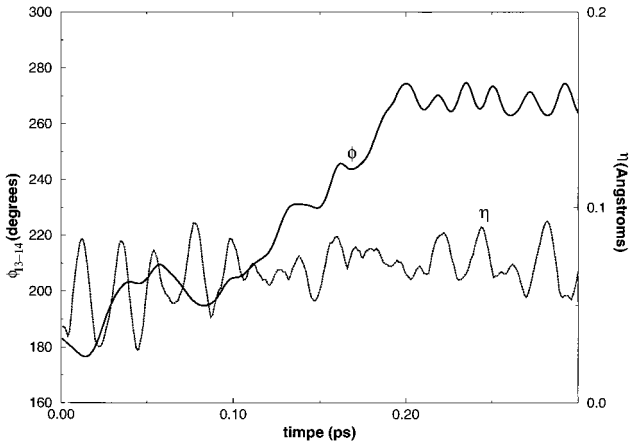

Figure 6. Time dependence of the torsional and the stretching motions for an excited-state trajectory of bR. The combined stretching coordinate η is defined by eq 18.

(relative to in a vacuum) than in bR (e.g., see section V.4 of ref 74) and that the differential blue shift will contribute to the calculated red shift in the spectrum of bR, relative to the spectrum of PSBR in solution. An additional shift may be because the chromophore in bR is in the 6→7 trans configuration, whereas PSBR in solution has a cis configuration. However, a careful examination of the issue would require systematic simulations of the spectrum of PSBR in solution (this should also include comparative study of the effect of different counterions[69,70]). Such a study is out of the scope of the present work.

Set II, which was optimized with the requirement of obtaining a proper quantum yield (see below), produced an absorption maximum at 23 300 cm^{-1}. A better refinement that would lead to a simultaneous reproduction of proper quantum yield and better absolute value for the excitation energy is clearly possible, but it is left for subsequent works.

III.2. Motion toward the Surface Crossing Region. As stated above, we started the excited trajectory in the Franck−Condon region by using coordinates and momenta which were selected from arbitrary points along the ground state trajectory. Here, as in our treatment of the surface hopping process, it is possible to treat the nuclear motion on a more "quantum mechanical level" (see discussion for rigorous treatment in simple cases in ref 76). However, our results are not expected to drastically depend on the initial conditions, because the kinetic energy of the torsional model tends to undergo very fast relaxation to other degrees of freedom (see below). At any rate, the nature of a typical excited-state trajectory, which was evaluated with set II, is depicted in Figure 4 (similar results were obtained using set I although in this case the system is trapped at $\phi < 270°$). As seen from the figure, the molecule moves in a diffusive rather than inertial motion. That is, the motion of trajectories that are *not* allowed to cross to the ground state can be classified as inertial or diffusive. The inertial motion is characterized by large-amplitude oscillations at the $\pi/2$ region, because the energy will stay at the original torsional coordinate. The diffusive motion is characterized by small random oscillations at the $\pi/2$ regions; in this case, the torsional kinetic energy is transferred very rapidly to other degrees of freedom (as is the case in Figure 3 of ref 19). Obviously, the results presented in the figure correspond to a diffusive motion. It should be noted that we do not allow surface crossing in analyzing the excited-state motion because the oscillations at the $\pi/2$ region (which would not persist when surface crossing

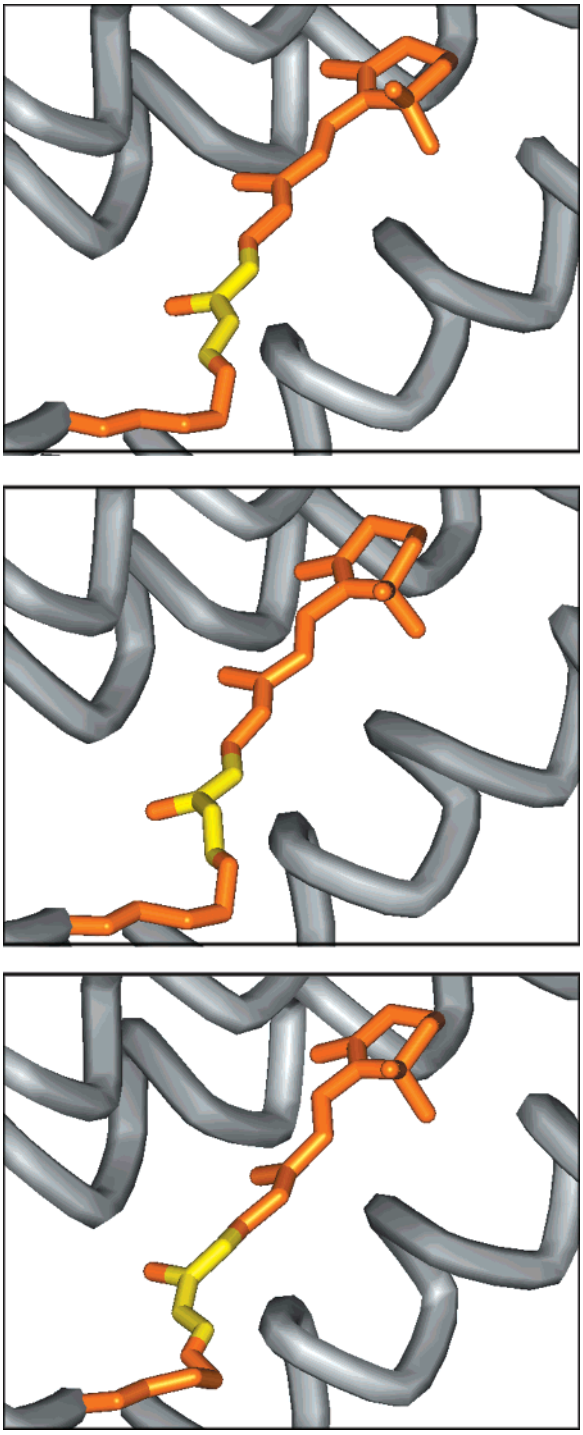

Figure 7. Snapshots from a typical surface-crossing trajectory of bR. The structures shown correspond to 0.0, 0.1, and 0.15 ps where the values of ϕ_{13-14} are 180°, 270°, and 320°, respectively.

is allowed) provide the simplest way of analyzing the excited motion in terms of a stochastic harmonic oscillator.[77] Such an analysis, which was reported in ref 19, has shown that we are dealing with a damped harmonic oscillator.

The fact that we do not have an inertial motion allows us to eliminate several models for the primary event even without any actual surface crossing calculations (see ref 19). For example, we can exclude the inertial model of Birge and Hubbard,[14] where the large oscillatory motion on the excited state determines the quantum yield (Figure 5a), because we have shown above that the torional motion is not inertial. We can also exclude a model where the crossing point is located

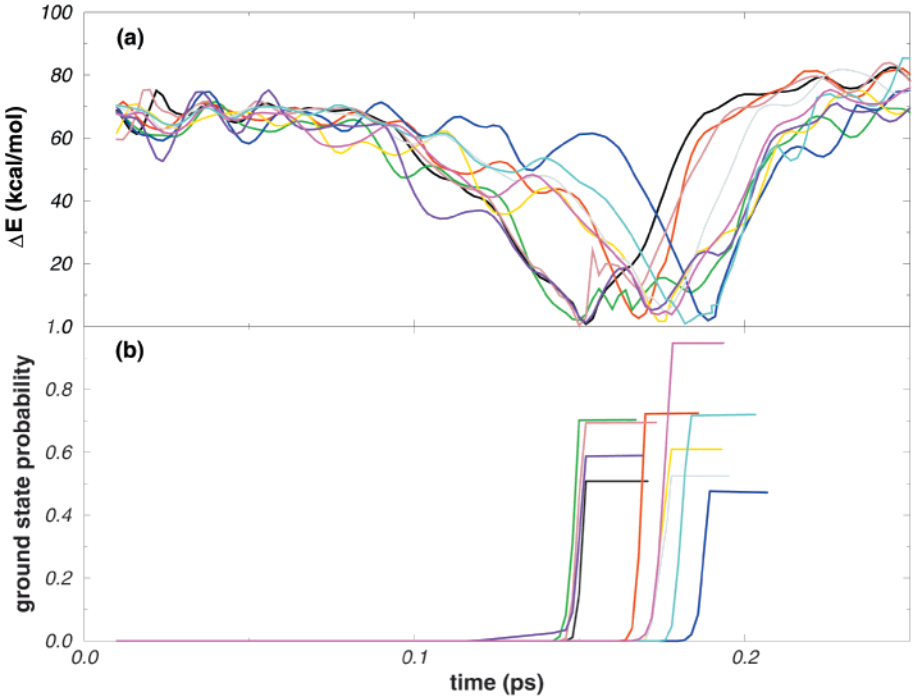

Figure 8. (a) Time dependence energy gaps, ΔW, for 10 trajectories that start on the excited-state surface at the Franck−Condon region and cross to the ground state at $\pi/2$. (b) The crossing probabilities $|a_0|^2$ for the trajectories with the above energy gaps. These probabilities correspond to $P_1(r_1)$ in eq 5 and are kept constant after the trajectory, $r_1(t)$, leaves the crossing region (see text).

significantly before the $\pi/2$ region (here we refer interchangeably to $\pi/2$ and $-\pi/2$), because in this case the system will equilibrate on the excited state and most trajectories will end up at the trans ground state (Figure 5b). The situation presented in Figure 5b is a limiting case of the results obtained by set I. That is, the use of set I leads to conical intersections before and after the $\pi/2$ region. Here again, it is likely that many trajectories that cross before the $\pi/2$ region will be deflected back to the trans region. This situation will be explored in section III.5.

Another interesting issue is the nature of the motion immediately after excitation. This issue is explored in Figure 6, where we present the time dependence of the collective bond stretching mode (see ref 78).

$$\eta = \sum_{i=1}^{m} |\Delta b_i|/m \qquad (19)$$

where $\Delta b_i = b_i - b_i^0$ (here b_i^0 is the ground-state length of the ith bond) and i runs over all of the π bonds. As seen from the figure, we have fast bond stretching oscillations before we start to have a torsional motion. This interesting feature is consistent with recent calculations[34] and experimental studies.[79−82] Interestingly, the fact that the initial motion on the excited-state surface involves bond stretching modes has already been detected in our original simulations,[6] where these motions were identified as the oscillation on the time dependent potential surface for the downhill trajectory (Figure 3 of ref 6).

III.3. Nature of the Crossing Process. The probability of crossing from the excited state to the ground state was examined for the two limiting cases of sets I and II. We started with set II, which we consider to be much more realistic (see below). The simulation was done by propagating trajectories on the excited state and letting them cross to the ground state at the $\pi/2$ point, where we conserved energy according to eq 6. Snapshots from the coordinates generated in a typical trajectory are depicted in Figure 7, whereas the $\Delta E(t)$ and crossing probabilities for 10 surface hopping trajectories are summarized in Figure 8. As seen from the figure, some trajectories have small enough ΔE to be classified as being at the immediate neighborhood of conical intersections (i.e., $|\Delta E| < 2$ kcal/mol). Other trajectories involve larger ΔE and large σ. The large σ might well reflect the presence of a nearby conical intersection, but as explained in the Introduction, it is consistent with what was found in our early studies. The actual distance from our crossing points to the closest conical intersections can be examined by searching these intersections using the gradient of the energy gap.[28] Such an analysis is left, however, for subsequent studies.

We also examined the surface crossing for the limiting case obtained by the parameters of set I. Here, we obtained more cases which can be classified as crossing through strict conical intersections. However, most of these trajectories returned on the ground state to the trans region. This point is illustrated in the upper and lower parts of Figure 9 which describe the time dependence of ϕ_{13-14} for trajectories on the surfaces of sets I and II, respectively. In the case of set II, all 10 trajectories continued after the crossing to the ground state, toward the cis direction (with a larger set of trajectories we found that a few crossed back). On the other hand, in the case of set I, 9 out of 10 trajectories were deflected back to the trans direction after crossing to the ground sate before the $\pi/2$ region.

III.4. How Exact Should the Surface Hopping Process Be Treated? Our surface hopping approach involves the reasonable approximation of eq 6. However, as stated in section II, semiclassical treatments cannot give the exact result for the quantization of the nuclear coordinate. Thus, instead of finding a "better" approximation, we tried here to use a very bad approximation and to show that even in this case one obtains results which are similar to those obtained with eq 6. This was done by repeating calculations, while keeping the excited-state trajectories on the excited-state surface after they pass the $\pi/2$ point. The corresponding $|a_0|^2$ was evaluated at the first turning

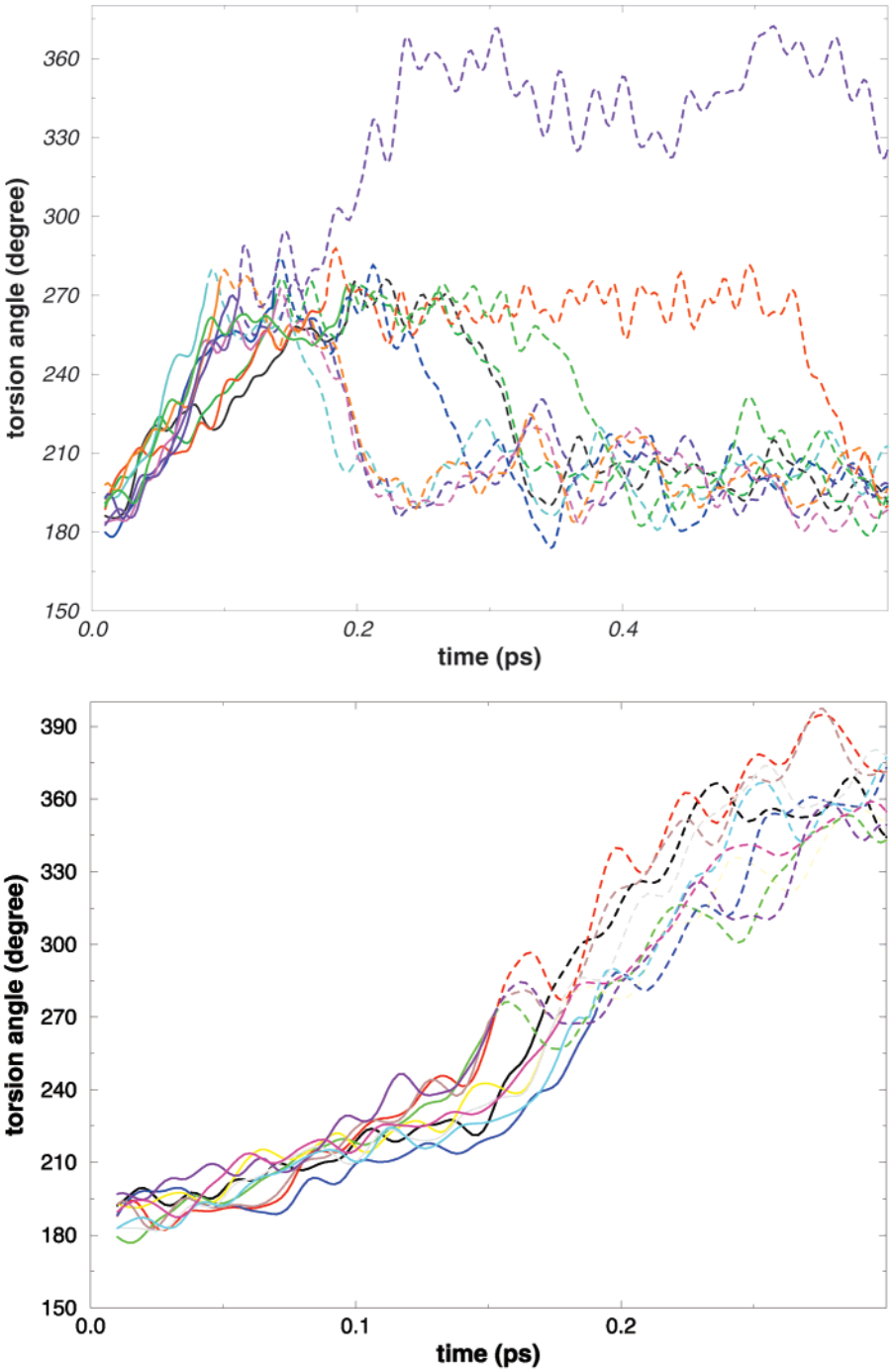

Figure 9. Showing the change of ϕ_{13-14} for surface crossing trajectories with the potential surfaces of set I (upper figure) and set II (lower figure). The trajectories on the excited state and ground state are designated by (—) and (- - -), respectively. As seen from the figure, the trajectories on the surface of set I tend to be deflected backward to the trans direction.

point after the $\pi/2$ region. The crossing probabilities obtained in this way for 10 trajectories, on the surface of set II, are depicted in Figure 10. Apparently the results shown in Figure 10 are similar to those presented in Figure 8. This demonstrates that in the present case the calculated crossing probabilities are not extremely sensitive to the effective potential that determines the trajectories ($r(t)$) of the nuclear coordinates. Obviously, the proper treatment should involve crossing from E_1 to E_0 at some point in the $\pi/2$ region. However, even incorrect evaluation of the surface hopping process gives similar crossing probability to that obtained with more reasonable treatments. This means that our conclusion about θ are quite robust.

III.5. The Quantum Yield. After establishing the limited sensitivity of our results to the exact surface switching procedure we turned to evaluate the overall quantum yield. This was done by the procedure described in section II and eq 5, where we split the trajectories at the crossing points and collect the probabilities of ending at the cis or trans directions. Figure 11 demonstrates our approach by considering a single surface hopping simulation, and Figure 12 presents the behavior of the system in five surface hopping trajectories. All of these calculations were done with the parameters of set II. As seen from Figure 12, we have an average crossing probability (the initial raise in the cis probability) of about 0.66 ($\theta = 0.66$) and

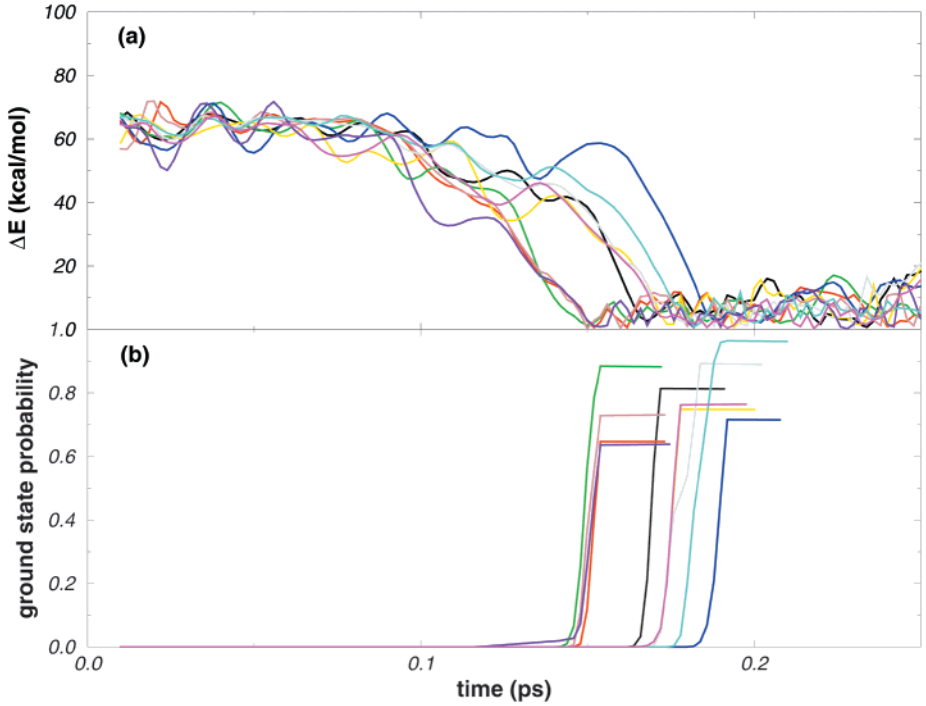

Figure 10. (a) Time dependence energy gaps for 10 trajectories that start on the excited state and were *not* allowed to cross. (b) The crossing probabilities $|a_0|^2$ for the trajectories with the above energy gaps. These probabilities correspond to the first pass at the $\pi/2$ region and are collected at the first turning point. This corresponds to P_1 in eq 5 except that r_1 is evaluated incorrectly and does not involve a crossing to the ground state. Comparing this figure to Figure 8 demonstrates that $|a_0|^2$ does not depend so strongly on whether r_1 continues (until the turning point) on E_1 or crosses to E_0.

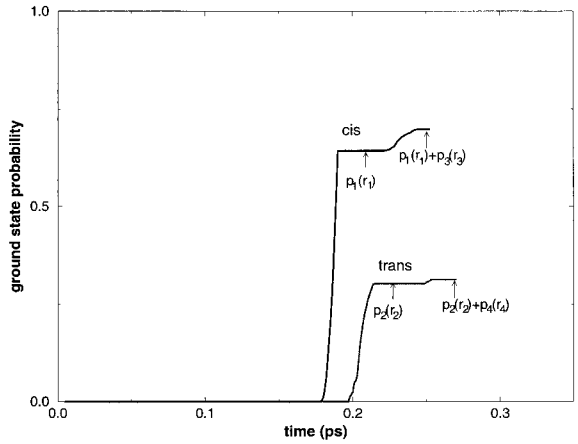

Figure 11. Accumulated probabilities of the cis and trans ground states for a single surface hopping trajectory. The $P_i(r_i)$ probabilities are defined and discussed in the text.

a final cis quantum yield of ~0.7 ($P_{cis} = 0.7$). This corresponds to a quantum yield of ~0.75 calculated from eq 1. Although our calculations slightly overestimate the observed quantum yield ($Y \cong 0.64$),[22,23] we find these results very encouraging. We note in this respect (see section III.3) that a small fraction of the trajectories that cross to the ground state in the cis direction are deflected back to the trans direction (even with set II). This type of behavior is expected to reduce Y, although trajectories that cross in the trans direction may be deflected to the cis direction.

As is clear from the discussion in section III.3 and Figure 9a the use of set I generates a model with a small quantum yield. Obviously such a model is inconsistent with the high quantum yield of bR.

Birge and co-workers,[1] who questioned the validity of our early studies, presented interesting studies of the photoisomerization in rhodopsin[14,15] and bR[1], using a simplified one-dimensional model which involved an isomerization around the primary bond (the $C_{11}-C_{12}$ and $C_{13}-C_{14}$ in rhodopsin and bR, respectively). The one-dimensional nature of the model forced these authors to introduce an arbitrary rate constant for the dissipation of the internal energy. The calculated rate of isomerization and quantum yield depended on the choice of this rate constant, because the excitation prepared the system with excess vibrational energy and the energy gap between the ground and excited states was assumed to decrease as this energy dissipated. This treatment neglects the possibility of transitions from excited vibrational levels of the excited electronic state to the same excited vibrational levels of the ground state (see discussion in ref 5). Relaxations of high-frequency vibrational modes of the chromophore (quantum modes) probably do not change the effective energy gap significantly. Relaxations of low-frequency (classical) vibrational modes occurs automatically in models that use more realistic multidimensional trajectories (e.g., ref 6 and the current work). At any rate, the calculations for bR[1] gave a quantum yield of ~0.27, whereas the observed value is ~0.64 (see refs 22 and 23).

Schulten and co-workers have described simulations of the photoisomerization of bR by a variety of computational approaches. Their recent studies[18] featured a model with three diabatic electronic states (S_a, S_b, and S_c), whose relative energies were assumed to depend on the $C_{13}-C_{14}$ dihedral angle (ϕ) as shown in Figure 13. The diabatic states were mixed by coupling factors that the authors assumed to be independent of ϕ. The diabatic energies and coupling factors were not calculated directly in this work, and no attempt was made to incorporate interactions with the protein explicitly; conjugation of the $C_{13}-C_{14}$ π electrons with the other π electrons of the chromophore also was not considered explicitly. The energies and coupling terms were chosen to make the energies of the resulting adiabatic states (S_0, S_1, and S_2 in our notation) resemble those obtained

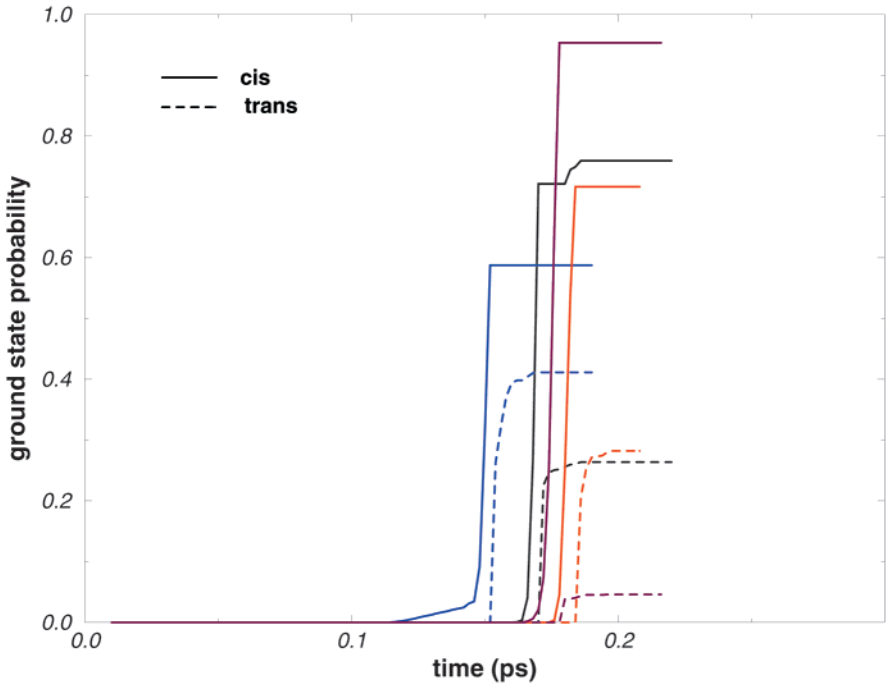

Figure 12. Accumulated probabilities of being in the ground state at the cis and trans regions for five surface hopping trajectories.

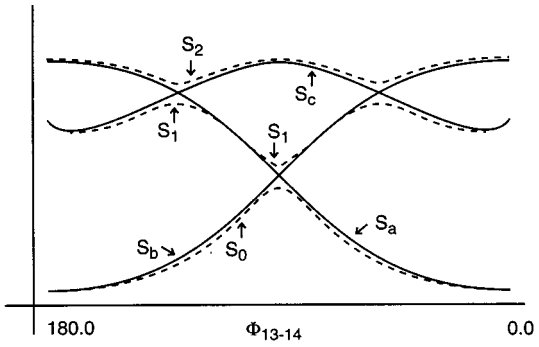

Figure 13. Three state model of the type used in ref 18 (see text for discussion).

in ab initio calculations for a PSBR analogue, but the separation of 4.4 kcal/mol between S_1 and S_2 at $\phi \sim 150°$ was much smaller than the gaps of 20−30 kcal/mol that Garavelli, Olivucci, and their colleagues[33,34] have obtained in high-level ab initio calculations for similar analogues (PDI and MNTI). As the authors noted, the assumed coupling of S_b and S_a ($\sigma_{ab} =$ 0.5 kcal/mol) was also considerably smaller than one would estimate based on the splitting of the ab initio energies at 90°.

The zero order diabatic wave functions and energies of the three-state-model of ref 18 do not necessarily provide an optimal basis set for the actual adiabatic picture of a double bond system (e.g., see ref 83). Furthermore, as much as the small barrier on the lowest adiabatic excited state is concern, the three-state-model does not seem to be qualified as a new model. That is, all of our models (e.g., see ref 6) have included many electronic states rather than just two states (although the physics is correctly described by the crossing between S_1 and S_0). Now, the calculated lowest adiabatic excited state, S_1, of the many states model of retinal and related molecules have frequently involved a small barrier to leaving the Franck−Condon region (e.g., see ref 21), although it has been pointed out repeatedly (e.g., Figure 3 of ref 21) that the protein electrostatic effect is likely to flatten this barrier (in the case of an isolated PSBR the barrier is already very small). In this respect, the difference between our potential surfaces and the model of ref 18 is that in the latter the two adiabatic excited states seem to come too close at $\phi = 150°$ (see above).

Using the three-state model, Ben-Nun et al.[18] propagated MD trajectories starting in diabatic state S_c at $\phi = 180°$. They followed the evolution of the system by the "full multiple spawning" (FMS) method, a quantum-mechanical formalism that allows a full numerical solution of the Schrödinger equation for a multidimensional Gaussian wave packet. About 48% of the population isomerized to the 13-cis ground state (S_a) with an apparent time constant of about 500 fs. However, about 51% was still in the excited state (S_c) when the trajectories were terminated at 1 ps; less than 1% was found in the 13-trans ground state (S_b). Although Ben-Nun et al. describe the simulations as giving isomerization on a time scale of 300 fs with a quantum yield of 0.48, an extrapolation of their results suggests that the ultimate quantum yield of S_a probably would be at least 0.95, considerably higher than the yield of 0.64 that is observed experimentally, and that the average time constant of the isomerization would be on the order of 1.5 ps (considerably longer than observed).

IV. Concluding Remarks

This work presented semiclassical simulation of the quantum dynamics of bR. The crossing probability and the relevant nonadiabatic coupling terms were calculated consistently from the QM/MM surface and wave function of the complete system. The nature of the calculated results obtained here with the actual protein environment are similar in many respects to that obtained in our original 1976 study with a very simplified model of the effect of rhodopsin.[6] Here, however, the availability of the actual protein structure lends more credibility to the calculations and allows us to examine such features as the "back" deflection of trajectories on the ground-state surface.

One of the main issues explored in this work is the nature of the surface crossing process. Although there is no way at present to obtain exact potential surfaces for such complex systems as bR, it seems from our study that different trajectories will have

different energy gap. This means that if some trajectories pass through "exact" conical intersections others involve nonzero energy gap and large nonadiabatic coupling. One may still argue correctly, that the large crossing probability reflect the neighborhood of conical intersections, but this is more a nice rationalization of the previous findings of large θ's and effective funnels[6,21] rather than a new picture of photobiological processes. The fact that some trajectories do not funnel through the exact $\Delta E = 0$ intersections is advantageous in terms of providing a robust biological system which will not be damaged by mutational changes (or other perturbations).

The fact that mutations that change the excited-state lifetime do not have significant effect on the quantum yield[22] was invoked as an evidence for a three state model.[12] However, as stated in section III.5, the three state model does not provide a new insight (unless S_1 and S_2 touch each other, which is not likely[83]). In fact, the explanation for the independence of the quantum yield on the excited-state lifetime is rather simple. That is, the quantum yield is determined by eq 1 and by the crossing probability at the $\pi/2$ region, whereas the excited-state lifetime (as measured by fluorescence from the $|\phi| < 50°$) region is determined by the shape of the surface for diffusion from $\phi \sim 60°$ to $\phi \approx \pi/2$. Some mutants may have a small barrier on this surface, or just make the surface more flat. This will increase the trajectory time as demonstrated in the computer experiment of ref 19. We believe that the very challenging experimental determination of the lifetime at $|\phi| > 70°$ will confirm our view.

The present work supports our early view[5] that some trajectories can be deflected backward on the ground state. This feature is particularly important in cases where the surface crossing occurs before the $\pi/2$ region (e.g., Figure 9a). Obviously, it is essential to consider such back-deflection in quantum yield calculations. Interestingly, it is not clear whether some surface crossing treatments (e.g., the FMS method of ref 18) can capture this effect. We believe that the simple physics of the surface hopping approach provides the most effective current way of following the position of the molecules on such complex multidimensional surfaces.

The present work started with the QCFF/PI surfaces which where calibrated by the gas phase ab initio potential surfaces of MNTI. However, the resulting QCFF/PI bR surfaces (set I) produced conical intersections before the $\pi/2$ region and thus a poor quantum yield. Adjusting the QCFF/PI QM/MM surface to give maximum crossing probability at the $\pi/2$ region, corrected this problem and allowed us to examine the nature of the surface crossing process. One may argue that our parametrization procedure biased the results of the model. However, it seems to us that what we obtain is a powerful tool for examining different mechanistic options. That is, changing set II within a reasonable range (while avoiding a model that leads to crossing before the $\pi/2$ region) produced quite robust results. For example, we could not force our model to produce surface crossings only at strict conical intersections. This result is not likely to change with more accurate surfaces. Similarly, the conclusion about the back deflection of trajectories that cross before the $\pi/2$ region is not likely to change in future simulations with more accurate potentials.

Finally, it might be useful to comment here on the role of the protein in controlling the photoisomerization of rhodopsins. It has been frequently suggested by us[5,6,21] and others[84] that the protein catalyzes the primary event by using its electrostatic effect to reduce the excited-state barrier and by using its steric effect to guide the isomerization about specific bonds. However, the confirmation of these catalytic proposals must involve comparative studies of the photoisomerization in solution and in the protein active site. Such a study is now underway in our lab.

Acknowledgment. This work was supported by NIH Grant GM-40283.

References and Notes

(1) Birge, R. R. Nature of the primary photochemical events in rhodopsin and bacteriorhodopsin. *Biochim. Biophys. Acta* **1990**, *1016*, 293−327.

(2) Lanyi, J. K.; Luecke, H. Bacteriorhodopsin. *Curr. Opin. Struct. Biol.* **2000**, *11*, 415-419.

(3) Mathies, R. A.; Brito Cruz, C. H.; Pollard, W. T.; Shank, C. V. Direct observation of the femtosecond excited-state cis−trans isomerization in bacteriorhodopsin. *Science* **1988**, *240*, 777−779.

(4) Warshel, A. Conversion of Light Energy to Electrostatic Energy in the Proton Pump of Halobacterium halobium. *Photochem. Photobiol.* **1979**, *30*, 285−290.

(5) Warshel, A.; Barboy, N. Energy Storage and Reaction Pathways in the First Step of the Vision Process. *J. Am. Chem. Soc.* **1982**, *104*, 1469.

(6) Warshel, A. Bicycle-Pedal Model for the First Step in the Vision Process. *Nature* **1976**, *260*, 679−683.

(7) Busch, G. E.; Applebury, M. L.; Lamola, A. A.; Rentzepis, P. M. Formation and decay of prelumirhodopsin at room temperature. *Proc. Natl. Acad. Sci. U.S.A.* **1972**, *69*, 2802−2806.

(8) Doukas, A. G.; Junnarkar, M. R.; Alfano, R. R.; Callender, R. H.; Kakitani, T.; Honig, B. Fluorescence quantum yield of visual pigments: Evidence for subpicosecond isomerization rates. *Proc. Natl. Acad. Sci. U.S.A.* **1984**, *81*, 4790−4794.

(9) Loppnow, G. R.; Mathies, R. A.; Middendorf, T. A.; Gottfried, D. S.; Boxer, S. G. Photochemical hole-burning spectroscopy of bovine rhodopsin and bacteriorhodopsin. *J. Phys. Chem.* **1992**, *96*, 737−745.

(10) Wang, Q.; Schoenlein, R. W.; Peteanu, L. A.; Mathies, R. A.; Shank, C. V. Vibrationally Coherent Photochemistry in the Femtosecond Primary Event of Vision. *Science* **1994**, *266*, 422.

(11) Nuss, M. C.; Zinth, W.; Kaiser, W.; Koelling, E.; Oesterhelt, D. Femtosecond spectroscopy of the 1st events of the photochemical cycle in bacteriorhodopsin. *Chem. Phys. Lett.* **1985**, *117*, 1−7.

(12) Hasson, K. C.; Gai, F.; Anfinrud, P. A. The photoisomerization of retinal in bacteriorhodopsin: Experimental evidence for a three-state model. *Proc. Natl. Acad. Sci. U.S.A.* **1996**, *93*, 15124−15129.

(13) Dobler, J.; Zinth, W.; Kaiser, W.; Oesterhelt, D. Excited-state reaction dynamics of bacteriorhodopsin studied by femtosecond spectroscopy. *Chem. Phys. Lett.* **1988**, *144*, 214−220.

(14) Birge, R. R.; Hubbard, L. M. Molecular dynamics of cis−trans isomerization in rhodopsin. *J. Am. Chem. Soc.* **1980**, *102*, 2195−2205.

(15) Tallent, J. R.; Hyde, E. W.; Findsen, L. A.; Fox, G. C.; Birge, R. R. Molecular Dynamics of the Primary Photochemical Event in Rhodopsin. *J. Am. Chem. Soc.* **1992**, *114*, 1581−1592.

(16) Logunov, I.; Schulten, K. Quantum chemistry: Molecular dynamics study of the dark-adaptation process in bacteriorhodopsin. *J. Am. Chem. Soc.* **1996**, *118*, 9727−9737.

(17) Xu, D.; Martin, C.; Schulten, K. Molecular dynamics study of early picosecond events in the bacteriorhodopsin photocycle: dielectric response, vibrational cooling and the J, K intermediates. *Biophys. J.* **1996**, *70*, 453−460.

(18) Ben-Nun, M.; Molnar, F.; Lu, H.; Philips, J. C.; Martinez, T. J.; Schulten, K. Quantum dynamics of the femtosecond photoisomerization of retinal in bacteriorhodopsin. *Faraday Discuss.* **1998**, *110*, 447−462.

(19) Warshel, A.; Chu, Z. T.; Hwang, J.-K. The Dynamics of the Primary Event in Rhodopsins Revisited. *Chem. Phys.* **1991**, *158*, 303−314.

(20) Birge, R. R.; Hubbard, L. M. Molecular dynamics of trans-cis isomerization in bathorhodopsin. *Biophys. J.* **1981**, *34* (3), 517−34.

(21) Weiss, R. M.; Warshel, A. A New View of the Dynamics of Singlet cis−trans Photoisomerization. *J. Am. Chem. Soc.* **1979**, *101*, 6131−6133.

(22) Logunov, S. L.; El-Sayed, M. A.; Song, L.; Lanyi, J. K. Photoisomerization quantum yield and apparent energy content of the K intermediate in the photocycles of bacteriorhodopsin, its mutants D85N, R82Q, and D212N, and deionized blue bacteriorhodopsin. *J. Phys. Chem.* **1996**, *100*, 2391−2398.

(23) Song, L.; El-Sayed, M. A.; Lanyi, J. K. Effects of changing the position and orientation of Asp85 relative to the protonated Schiff base within the retinal cavity on the rate of photoisomerization in bacteriorhodopsin. *J. Phys. Chem.* **1996**, *100*, 10479−10481.

(24) Titor, J.; Oesterhelt, D. The quantum yield of bacteriorhodopsin. *FEBS Lett.* **1990**, *263*, 269−273.

(25) Rosenfeld, T.; Honig, B.; Ottolenghi, M.; Hurley, J. B.; Ebrey, T. Cis−trans isomerization in the photochemistry of vision. *Pure Appl. Chem.* **1977**, *49*, 341−351.

(26) Persico, M.; Bonacic-Koutecky, V. Nonadiabatic coupling between low lying singlet states of geometrically relaxed olefines: Ethylene and propylene. *J. Chem. Phys.* **1982**, *76*, 6018.

(27) Michl, J., Photochemical Reactions of Large Molecules. I. A Simple Physical Model of Photochemical Reactivity. *Mol. Photochem.* **1972**, *4*, 243, 257, 287.

(28) Olivucci, M.; Ragazos, I. N.; Bernardi, F.; Robb, M. A. A Conical Intersection Mechanism for the Photochemistry of Butadiene. *J. Am. Chem. Soc.* **1993**, *115*, 3710−3721.

(29) Garavelli, M.; Bernardi, F.; Olivucci, M.; Vreven, T.; Klein, S.; Celani, P.; Robb, M. A. Potential-energy surfaces for ultrafast photochemistry. Static and dynamic aspects. *Faraday Discuss.* **1998**, *110*, 51−70.

(30) Klessinger, M. Conical Intersections and the Mechanism of Singlet Photoreactions. *Angew. Chem., Int. Ed. Engl.* **1995**, *34*, 549−551.

(31) Yarkony, D. R. Conical Intersections: diabolical and often misunderstood. *Acc. Chem. Res.* **1998**, *31*, 511−518.

(32) Teller, E. The crossing of potential surfaces. *J. Phys. Chem.* **1937**, *41*, 109−116.

(33) Garavelli, M.; Celani, P.; Bernardi, F.; Robb, M. A.; Olivucci, M. The $C_5H_6NH_2^+$ Protonated Shiff Base: An ab Initio Minimal Model for Retinal Photoisomerization. *J. Am. Chem. Soc.* **1997**, 119, 6891−6901.

(34) Garavelli, M.; Vreven, T.; Celani, P.; Bernardi, F.; Robb, M. A.; Olivucci, M. Photoisomerization path for a realistic retinal chromophore model: The nonatetraeniminium cation. *J. Am. Chem. Soc.* **1998**, *120*, 1285−1288.

(35) Desouter-Lecomte, M.; Galloy, C.; Lorquet, J. C.; Vaz Pires, M. Nonadiabatic interactions in unimolecular decay. V. Conical and Jahn−Teller intersections. *J. Chem. Phys.* **1979**, *71* (9), 3661−3672.

(36) Henderson, R.; Baldwin, J. M.; Ceska, T. A.; Zemlin, F.; Beckman, E.; Downing, K. H. Model for the Structure of Bacteriorhodopsin Based on High-resolution Electron Cryo-microscopy. *J. Mol. Biol.* **1990**, *213*, 899−929.

(37) Kimura, Y.; Vassylyev, D. G.; Miyazawa, A.; Kidera, A.; Matsushima, M.; Mitsuoka, K.; Murata, K.; Hirai, T.; Fujiyoshi, Y. Surface of bacteriorhodopsin revealed by high-resolution electron crystallography. *Nature* **1997**, *389*, 206−211.

(38) Luecke, H.; Schobert, B.; Richter, H.-T.; Cartailler, J.-P.; Lanyi, J. K. Structural changes in bacteriorhodopsin during ion transport at 2 angstrom resolution. *Science* **1999**, *286*, 255−260.

(39) Luecke, H.; Schobert, B.; Richter, H. T.; Cartailler, J. P.; Lanyi, J. K. Structure of bacteriorhodopsin at 1.55 angstrom resolution. *J. Mol. Biol.* **1999**, *291*, 899−911.

(40) Miller, W. H.; George, T. F. Semiclassical Theory of Electronic Transitions in Low Energy Atomic and Molecular Collisions Involving Several Nuclear Degrees of Freedom. *J. Chem. Phys.* **1972**, *56*, 5637−5652.

(41) Tully, J. C.; Preston, R. M. Semiclassical Trajectory Surface Hopping Approach to Nonadiabatic Molecular Collisions: The reaction of H^+ with D2. *J. Phys. Chem.* **1971**, *56*, 562−572.

(42) Jen, C. F.; Warshel, A. Microscopic Based Density Matrix Treatments of Electron-Transfer Reactions in Condensed Phases. *J. Phys. Chem. A.* **1999**, *103*, 11378−11386.

(43) Warshel, A.; Karplus, M. Semiclassical Trajectory Approach to Photoisomerization. *Chem. Phys. Lett.* **1975**, *32*, 11.

(44) Warshel, A. Dynamics of Reactions in Polar Solvents. Semiclassical Trajectory Studies of Electron-Transfer and Proton-Transfer Reactions. *J. Phys. Chem.* **1982**, *86* (12), 2218−2224.

(45) Warshel, A.; Hwang, J.-K. Simulation of the Dynamics of Electron-Transfer Reactions in Polar Solvents: Semiclassical Trajectories and Dispersed Polaron Approaches. *J. Chem. Phys.* **1986**, *84*, 4938−4957.

(46) Webster, F.; Rossky, P. J.; Friesner, R. A. Nonadiabatic Processes in Condensed Matter: Semiclassical Theory and Implementation. *Comput. Phys. Comm.* **1991**, *63*, 494−522.

(47) Pechukas, P. Time-Dependent Semiclassical Scattering Theory. I. Potential Scattering. *Phys. Rev.* **1969**, *181*, 161−185.

(48) Webster, F. J.; Schnitker, J.; Friedrichs, M. S.; Friesner, R. A.; Rossky, P. J. Solvation dynamics of the hydrated electron—a nonadiabatic quantum simulation. *Phys. Rev. Lett.* **1991**, *66*, 3172−3176.

(49) Gelbart, W. M.; Freed, K. F.; Rice, S. A. Internal rotation and the breakdown of the adiabatic approximation: many-phonon radiationless transititons. *J. Chem. Phys.* **1970**, *52*, 2460−2473.

(50) Bixon, M.; Jortner, J. Intramolecular radiationless transitions. *J. Chem. Phys.* **1968**, *48*, 715−726.

(51) Siebrand, W. Radiationless transitions in polyatomic molecules. I. Calculations of Franck−Condon factors. *J. Chem. Phys.* **1967**, *46*, 440−447.

(52) Siebrand, W. Radiationless transitions in polyatomic molecules. II. Triplet-ground-state transitions in hydrocarbons. *J. Chem. Phys.* **1967**, *47*, 2411−2422.

(53) Ito, H.; I'Haya, Y. The Electronic Structure of Naphthalene. *Theor. Chim. Acta*, **1964**, *2*, 247−257.

(54) Persico, M. The Role of Nonadiabatic Coupling and Sudden Polarization in the Photoisomerization of Olefins. *J. Am. Chem. Soc.* **1980**, *102*, 7839−7545.

(55) Dormans, G. J. M.; Groenenboom, G. C.; van Dorst, W. C. A.; Buck, H. M. A quantum chemical study on the mechanism of cis trans isomerization in retinal-like protonated Schiff bases. *J. Am. Chem. Soc.* **1988**, *110*, 1406−1415.

(56) Kikuchi, H.; Suzuki, H. Dynamical theory of photoisomerization of the rhodopsin chromophore: generation of a transient electric field during photoisomerization. *J. Phys. Chem. B* **1997**, *101*, 6050−6056.

(57) Warshel, A.; Lappicirella, A. Calculations of Ground-and Excited-State Potential Surfaces for Conjugated Heteroatomic Molecules. *J. Am. Chem. Soc.* **1981**, *103*, 4664.

(58) Warshel, A.; Karplus, M. Calculation of π π^* Excited State Conformations and Vibronic Structure of Retinal and Related Molecules. *J. Am. Chem. Soc.* **1974**, *96*, 5677.

(59) Lee, F. S.; Chu, Z. T.; Warshel, A. Microscopic and Semimicroscopic Calculations of Electrostatic Energies in Proteins by the POLARIS and ENZYMIX Programs. *J. Comput. Chem.* **1993**, *14*, 161−185.

(60) Luzhkov, V.; Warshel, A. Microscopic Calculations of Solvent Effects on Absorption Spectra of Conjugated Molecules. *J. Am. Chem. Soc.* **1991**, *113*, 4491−4499.

(61) Warshel, A.; Levitt, M. *QCFF/PI: A Program for the Consistent Force Field Evaluation of Equilibrium Geometries and Vibrational Frequencies of Molecules.* QCPE 247, Quantum Chemistry Program Exchange; Indiana University: Bloomington, IN, 1974.

(62) Muller, M. G.; Hohlneicher, G. Prediction by AM1 of More Reasonable Geometries for 1,2-Diphenylcycloalkenes Than by Other Semiempirical MO Methods. *J. Am. Chem. Soc.* **1990**, *112*, 1273−1274.

(63) Reference 62 has compared the performance of the QCFF/PI to that of other methods including AM1. The results presented (which appear to be in contrast with the authors conclusions) indicate that the QCFF/PI provides the most reliable structures for sterically hindered conjugated molecules. This is apparent from examination of the calculated and observed values of the angles Ω and θ, while noting that the calculated potential minima must correspond to θ values which are smaller than the corresponding observed values (that reflect thermal average over a very flat and anharmonic potential).

(64) King, G.; Warshel, A. A Surface Constrained All-Atom Solvent Model for Effective Simulations of Polar Solutions. *J. Chem. Phys.* **1989**, *91* (6), 3647−3661.

(65) Lee, F. S.; Warshel, A. A Local Reaction Field Method for Fast Evaluation of Long-Range Electrostatic Interactions in Molecular Simulations. *J. Chem. Phys.* **1992**, *97*, 3100−3107.

(66) Warshel, A.; Papazyan, A. Electrostatic Effects in Macromolecules: Fundamental Concepts and Practical Modeling. *Curr. Opinion Struct. Biol.* **1998**, *8*, 211−217.

(67) Nonella, M. Electrostatic Protein-Chromophore Interactions Promote the all-trans-13-cis Isomerization of the Protonated Retinal Schiff Base in Bacteriorhodopsin: An ab Initio CASSCF/MRCI Study. *J. Phys. Chem. B* **2000**, *104*, 11379−11388.

(68) Ben Nun et al.[18] attempted to study the primary event in bR using a simple three-state model where the π electron energy was taken only as function of the ϕ_{13-14} torsional angle. This model, which used somewhat arbitrary coupling terms, has not considered the coupling between the chromophore and the protein electrostatic potential. Talnet et al.[15] used 1-D surfaces and represented the protein by the Lys residue that forms the Schiff base and by an external point charge. The steric effects of the Lys residue would have relaxed in more realistic calculations and the effect of the counterion would have been drastically reduced by protein dielectric effect. This effect is introduced and treated consistently in our QM/MM treatment, which includes the protein−solvent electrostatic interactions and the proper microscopic dielectric effect.

(69) Baasov, T.; Sheves, M. On the Absorption Maxima of Protonated Retinal Schiff Bases. An Interaction with External Charges. *Isr. J. Chem.* **1985**, *25*, 53−55.

(70) Baasov, T.; Sheves, M. Model Compounds for the Study of Spectroscopic Properties of Visual Pigments and Bacteriorhodopsin. *J. Am. Chem. Soc.* **1985**, *107*, 7524−7533.

(71) Logunov, I.; Schulten, K. Quantum Chemistry of in situ Retinal: Study of the Spectral Properties and Dark Adaptation of Bacteriorhodopsin. In *Quantum Mechanical Simulation Methods for Studying Biological Systems*; Bicout, D., Field, M., Eds.; Springer: Berlin, Germany, 1995.

(72) Nakanishi, K.; Balogh-Nair, V.; Arnadboldi, M.; Tsujimoto, K.; Honig, B. An External Point-Charge Model for Bacteriorhodopsin To Account for Its Purple Color. *J. Am Chem. Soc.* **1980**, *102*, 7945−7947.

(73) Warshel, A.; Ottolenghi, M. Kinetic and Spectroscopic Effects of Protein-Chromophore Electrostatic Interactions in Bacteriorhodopsin. *Photochem. Photobiol.* **1979**, *30*, 291.

(74) Warshel, A.; Russell, S. T. Calculations of Electrostatic Interactions in Biological Systems and in Solutions. *Q. Rev. Biophys.* **1984**, *17*, 283−421.

(75) Warshel, A. Calculations of Chemical Processes in Solutions. *J. Phys. Chem.* **1979**, *83*, 1640−1650.

(76) Warshel, A.; Hwang, J.-K. Quantized Semiclassical Trajectory Approach for Evaluation of Vibronic Transitions in Anharmonic Molecules. *J. Chem. Phys.* **1985**, *82*, 1756.

(77) Wang, M. C.; Uhlenbeck, G. E. On the theory of the Brownian motion II. *Rev. Mod. Phys.* **1945**, *17*, 323−342.

(78) Warshel, A. Charge Stabilization Mechanism in the Visual and Purple Membrane Pigments. *Proc. Natl. Acad. Sci. U.S.A.* **1978**, *75*, 2558.

(79) Delaney, J. K.; Brack, T. L.; Atkinson, G. H.; Ottolenghi, M.; Steinberg, G.; Sheves, M. Primary picosecond molecular events in the photoreaction of the BR512 artificial bacteriorhodopsin pigment. *Proc. Natl. Acad. Sci. U.S.A.* **1995**, *92*, 2101−2105.

(80) Kochendoerfer, G. G.; Mathies, R. A. Spontaneous emission study of the femtosecond isomerization dynamics of rhodopsin. *J. Phys. Chem.* **1996**, *100*, 14526−14532.

(81) Haran, G.; Morlino, E. A.; Matthes, J.; Callender, R. H.; Hochstrasser, R. M. Femtosecond polarized pump−probe and stimulated emission spectroscopy of the isomerization reaction of rhodopsin. *J. Phys. Chem. A* **1999**, *103*, 2202−2207.

(82) Song, L.; El-Sayed, M. A. Primary step in bacteriorhodopsin photosynthesis: Bond stretch rather than angle twist of its retinal excited-state structure. *J. Am. Chem. Soc.* **1998**, *120*, 8889−8890.

(83) Gonzalez-Luque, R.; Garavelli, M.; Bernardi, F.; Merchan, M.; Robb, M. A.; Olivucci, M. Computational Evidence in Favor of a Two-State Two-Mode Model of the Retinal Chromophore Photoisomerization. *Proc. Natl. Acad. Sci. U.S.A.* **2000**, *97*, 9379−9384.

(84) Logunov, S.; Song, L.; El-Sayed, M. Excited-state dynamics of a protonated retinal schiff base in solution. *J. Phys. Chem.* **1996**, *100*, 18586−18591.